www.DeepakPublishing.com

Védie N., et al. (2013): JoSS, Vol. 2, No. 1, pp. 119-131
(Peer-reviewed Article available at www.jossonline.com)

www.JoSSonline.com

Autonomous Ocean Current Geolocation from Orbit

Nathalie Védie[1], David A. Spencer[1], Luke Walker[1], and Michael S. Veto[2]

[1] *Georgia Institute of Technology, School of Aerospace Engineering, Atlanta, GA USA*
[2] *Arizona State University, School of Earth and Space Exploration, Tempe, AZ USA*

Abstract

A small satellite mission concept for the identification and tracking of ocean surface thermal features associated with warm-water currents is currently being developed within the Center for Space Systems at the Georgia Institute of Technology. The Ocean Thermal Imaging (OTI) mission will acquire thermal images using an uncooled focal plane array (UFPA), and apply on-board image processing algorithms to detect and geolocate warm-water ocean currents. A "blobber" algorithm is used to identify a set of contiguous pixels with characteristics that fall within specified temperature and area parameters. Satellite position and attitude knowledge are used to geolocate the thermal features. The resulting mission data products will provide a useful resource for the oceanographic science and maritime operations communities. This article gives an overview of the mission concept, introduces the microbolometer thermal imaging system, describes the design and testing of the thermal image processing algorithm, and discusses the process for the geolocation of thermal features.

1. Introduction

Ocean surface temperature measurements can be used to detect and track the location of warm-water currents. Knowledge of the time-varying locations of ocean surface currents has applications spanning chemical plume tracking, weather forecasting, and maritime operations. Presently, coastal currents are monitored through buoys, moorings, shore-based radar observations, and satellite altimetry, in addition to sea surface temperature mapping. The primary advantage of sea surface temperature observations is the near real-time determination of warm-water current locations.

The April 2010 Deepwater Horizon oil drilling rig disaster in the Gulf of Mexico dramatically highlighted the need for accurate monitoring of coastal currents in order to predict oil plume propagation for environmental response planning. Forecasting the trajectory of the Deepwater Horizon oil plume was complicated by

the lack of predictability of the behavior of the Loop Current, the largest warm-water current in the Gulf of Mexico. Entrainment of the oil in the Loop Current could have resulted in the plume being swept through the Florida Keys and into the Gulf Stream, which could have carried the oil up the southeastern coast of the United States with major ecological and economic consequences. Seasonal and day-to-day variations in the Loop Current complicate modeling efforts and emphasize the need for frequent observations (Leben and Born, 1993). Sea-surface temperature observations provide a critical data set for tracking the Loop Current, Gulf Stream, and warm-water current systems worldwide.

Near real-time knowledge of ocean current locations can enable maritime operations such as cargo ships, tankers and cruise vessels to optimize their courses based upon ocean current behavior. This would improve fuel efficiency and transfer times, as studies indicate that proper use of current forecast data can reduce cross-ocean transit times by up to one-to-two hours per day and reduce fuel consumption by up to eight percent (Davidson et al., 2009).

In Section 2 of this article, the Ocean Thermal Imaging (OTI) mission and spacecraft design are described, and Section 3 provides an overview of the microbolometer thermal imaging system that will be flown on the mission. The on-board image processing algorithm is described in Section 4, and the approach for thermal feature geolocation is discussed in Section 5. Summary conclusions are provided in Section 6.

1. Ocean Thermal Imaging Mission Overview

The OTI mission is designed to acquire thermal images using a UFPA, and apply on-board image processing algorithms to detect and geolocate warm-water ocean currents. The location and time-history of warm-water ocean features will be published to an online database, for use by the oceanographic science and maritime operations communities. Mission goals are to register the locations of selected warm-water currents twice per day, and make them publicly available within 12 hours of image acquisition. Ocean current geolocation errors shall be less than 1 km, including all error sources. The OTI mission concept is currently being developed within the Center for Space Systems at the Georgia Institute of Technology. An illustration of the OTI spacecraft is shown in Figure 1.

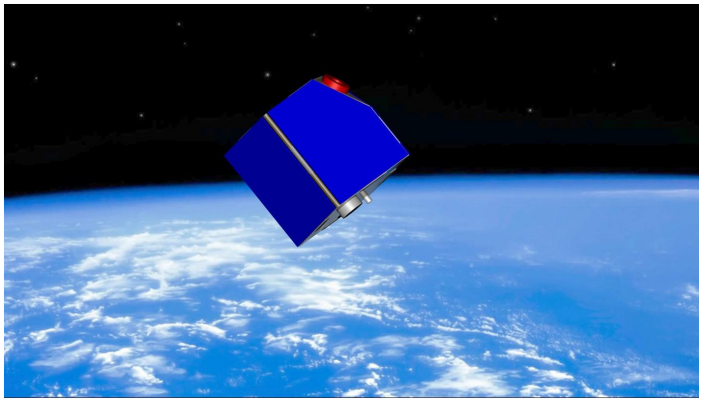

Figure 1. The OTI mission provides a small satellite approach to tracking warm-water ocean currents.

The 50 kg OTI satellite is constrained to have external dimensions within a volume of 50 x 50 x 60 cm, and is designed for launch as a secondary payload using the Expendable Secondary Payload Adapter (ESPA) interface. While the reference orbit altitude is 500 km, orbital altitudes from 385 km to 1,000 km can be accommodated. The 385 km lower altitude limit is defined by a six-month minimum mission duration requirement; lower altitudes may lead to orbit decay and re-entry within six months. The 1,000 km higher altitude limit is based upon a maximum orbit lifetime of 25 years. An orbit inclination of 34 degrees or greater is required for suitable tracking station coverage. Higher inclinations are desired, to allow observation of mid-latitude ocean currents. Spacecraft tracking will be provided by the Georgia Institute of Technology in Atlanta, Georgia (33.75° N, 84.4° W). Additional tracking stations will be identified, as needed.

The three-axis stabilized OTI satellite will acquire thermal images (range within 8 to 12 microns, due to optics limitation) using a microbolometer thermal imaging system consisting of an uncooled focal plane array and refractive optics (Walker and Spencer, 2010). From the reference orbit altitude of 500 km, the microbolometer thermal imaging system has a 79 km x 60 km swath, with a pixel size of 123 m x 125 m. Spatial

resolution scales linearly with altitude, to 250 m/pixel at the maximum orbit altitude of 1,000 km. Visible context images will also be acquired (range within 390 to 750 nm). The visible images are 1384 by 1032 pixels. The total footprint will be 127*95 km at a 500 km altitude and a pixel size of 92 m. OTI will demonstrate rapid on-board processing of the thermal images, to identify and geolocate features of interest. High-priority regions can be imaged as frequently as twice per day. The OTI satellite is data volume-limited, because of downlink data rates and tracking station overflight opportunities. For worst-case orbit geometries, a single pair of visible and infrared images can be downlinked per orbit. This limited data downlink capability drives the need for automated on-board processing of images. Thermal feature locations from processed images can be compressed and downlinked efficiently; OTI can process and downlink thermal feature locations from hundreds of images daily.

2.1 Spacecraft Overview

The OTI spacecraft is based upon a straightforward system design using flight-proven components that are tested at the subsystem and system level prior to launch. The design is inherited from the University Nanosat Program-7 (UNP-7) Prox-1 satellite, which is in the integration and testing phase at this time. All OTI components are at technology readiness level (TRL) 7 or above, with the exception of the advanced micro-sun sensors, which are at TRL-5. The spacecraft wet mass of 46.6 kg provides 7.7 percent launch mass margin with respect to the 50 kg maximum spacecraft launch mass allocation.

OTI is 3-axis stabilized with body-mounted solar arrays, UHF receiver and S-Band transmitter for communications. The system block diagram is shown in Figure 2. The external dimensions of OTI are 46 x 46 x 50 cm, providing volumetric margin relative to the

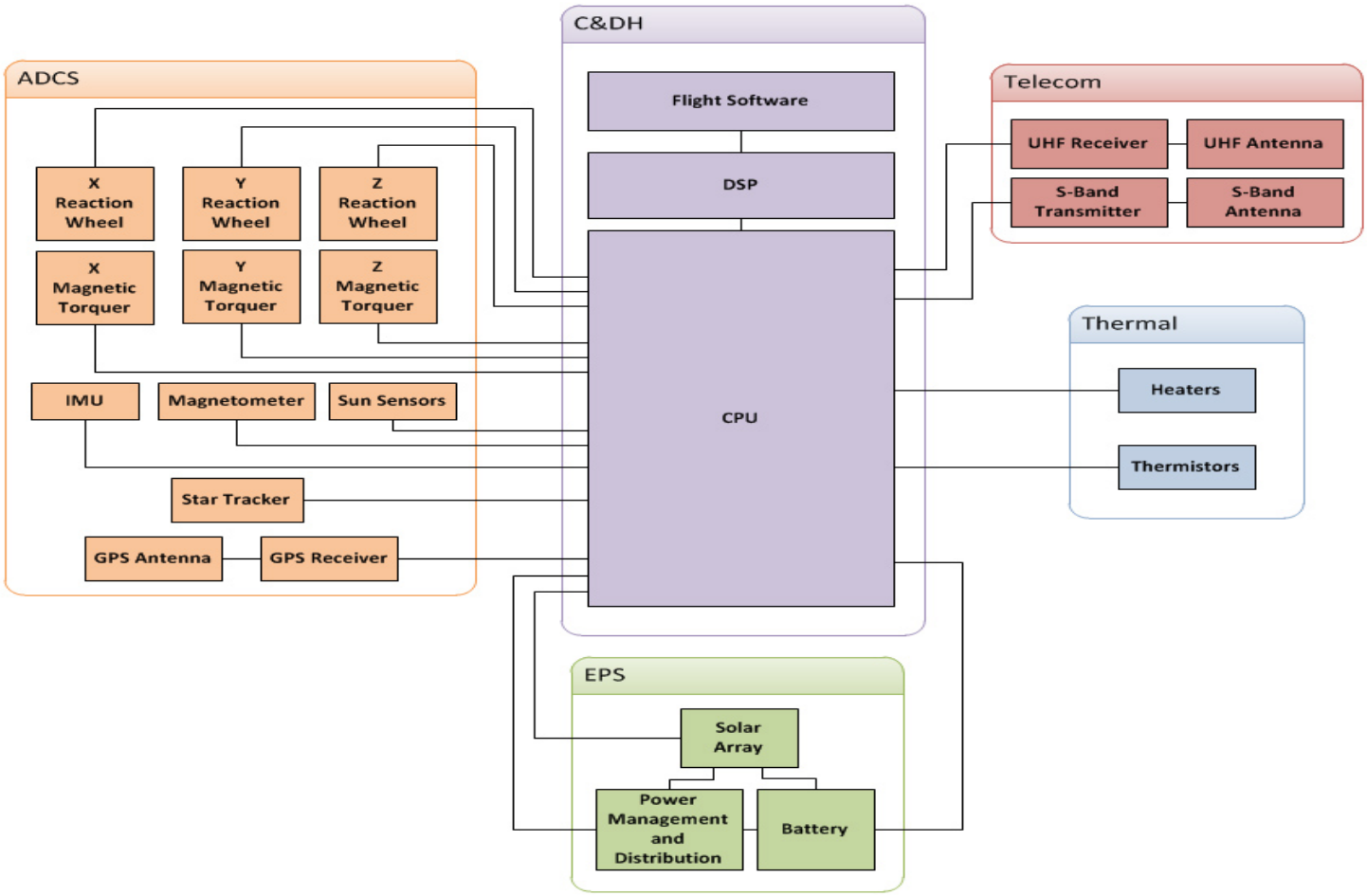

Figure 2. OTI spacecraft block diagram.

ESPA constraints. The aluminum spacecraft structure is sized to carry the launch loads and provide a stable platform for maneuvering and imaging operations. Orbit determination is provided via a GPS receiver. The attitude determination and control system includes a star tracker, sun sensors, an inertial measurement unit, and a magnetometer for attitude sensing, and torque rods and reaction wheels for attitude control. The flight computer is an off-the-shelf central processing unit and digital signal processor that provides command and data interfaces to the science instruments and spacecraft subsystems. Four GB of non-volatile memory and 512 MB of RAM provide ample science data storage margin. Lithium-ion battery cells provide power during eclipse periods. Thermal control is largely passive, consisting of multi-layer insulation and white paint, although active heaters are used when required.

In order to perform thermal imaging from a small spacecraft, a commercial off-the-shelf (COTS) UFPA provided by Raytheon Vision Systems is adapted for space application (Raytheon data sheet, 2008, 2010). A Point Grey Research Grasshopper visible camera will provide context for the thermal images (Point Grey Research Grasshopper, 2008).

2.2 Structures

The structure for the Prox-1 satellite is based upon a rectangular prism with dimensions 46 x 46 x 50 cm made from Aluminum 6061 plates. The first natural frequency is required to be greater than 100 Hz; compliance with this requirement is verified through finite element modeling and vibration testing of the structure. The OTI structure is a build-to-print of the Prox-1 design, which has been fabricated and vibration-tested.

2.3 Attitude Determination and Control

The driving requirements for the attitude determination and control subsystem (ADCS) are to: (1) damp initial attitude rates following launch vehicle separation; (2) acquire and maintain attitude reference, and (3) maintain precise pointing during normal operations.

Attitude determination during safe mode operations will be provided by a magnetometer and sun sensors. The Billingsley Aerospace & Defense TFM65-VQS magnetometer is baselined. OTI will flight-qualify new sun sensor technology that has been developed at the Jet Propulsion Laboratory for microsatellite applications. As shown in Figure 3, the advanced micro-sun sensor (AMSS) is a miniaturized pinhole camera using an Active Pixel Sensor camera on a chip, including optics that incorporate a silicon wafer with an evaporated layer of chrome and an additional gold layer with a number of small pinholes. The AMSS performs centroid calculations of the individual images, and outputs only the centroid positions and brightness to minimize the dataflow from the sensor. Processing is implemented in a single Field-Programmable Gate Array (FPGA), to minimize mass and power consumption. OTI will advance the AMSS from TRL-5 to TRL-9.

Figure 3. Advanced micro-sun sensor.

Attitude control during safe mode is provided by three orthogonally-oriented torque rods. The torque rods will react with the Earth's magnetic field to adjust the attitude of the satellite. The torque rods will provide up to 10 Am^2 linear dipole moment, which is sufficient for controlling the attitude of the satellite. Torque rods will be fabricated at Georgia Tech using the Prox-1 design.

Attitude determination during normal operations is provided by a star tracker. Commercially available star trackers are being evaluated for the OTI mission.

Attitude control is provided by three Maryland Aerospace MAI-400A reaction wheels. Each wheel provides a torque capability of 0.625 mN m, and has a maximum wheel speed of 10,000 rpm. Torque rods will be used to desaturate the reaction wheels. A Global Position System (GPS) unit will provide orbit determination. The SpaceQuest Ltd. GPS-12-V1 will provide high-rate orbital state and timing information that is filtered and utilized in the attitude determination process. Position accuracy of the GPS unit is specified as 10 m, and velocity accuracy is 0.03 m s^{-1} RMS.

2.4 Electrical Power Subsystem

The driving requirement for the electrical power subsystem (EPS) is to provide an average power of 28 W to the spacecraft during normal operations. Using body-mounted solar cells for power production and lithium-ion batteries for power storage, the EPS provides power management, distribution and conditioning throughout the mission.

The solar panels will be manufactured at Georgia Tech using Spectrolab Double Junction (DJ) solar cells, with a beginning-of-life efficiency of 21.5%. The solar panels will generate 54 W of power to 99% confidence based upon Monte Carlo analysis of spacecraft attitude and orbit geometry. A sun-regulated bus distributes power from the solar cells and batteries to the loads, with a nominal bus voltage of 28 +/- 1.5 VDC. During sunlight, shunt control dissipates excess power. Voltage is regulated to 5, 7, 12, 24 and 28 V for instrument and subsystem operation.

2.5 Command and Data Handling

The driving requirements for the command and data handling (C&DH) subsystem are to monitor the health and safety of the engineering subsystems, execute flight software operations, and command and telemetry data processing.

The flight computer is an off-the-shelf ARM-A8 Cortex central processing unit and TI C64x+ digital signal processor that provides command and data interfaces to the science instruments and spacecraft subsystems. Four GB of non-volatile memory and 512 MB of RAM provide ample science data storage margin. Subsystem micro-controllers are used for low-level analog-to-digital and digital-to-analog conversions.

The flight software is programmed in C/C++, and is run on the Micro-C OS/II operating system. The flight software architecture is modular by design, with separate tasks controlling high-level behaviors (e.g., health management, safe mode) and component-level functions (e.g., image acquisition, engineering data collection). Flight software algorithms are developed and tested in MATLAB™, and deliveries are made to the flight software development team for flight coding. New versions of flight software are run through a regression test suite to ensure the software integrity.

2.6 Telecommunications

The driving requirement of the telecommunications subsystem is to provide dependable uplink and downlink of all mission data, telemetry, and commands between the spacecraft and the ground station. A 500 km circular orbit with a 50 degrees inclination is used as a representative baseline for the potential orbits into which OTI could be launched, and overflight durations were determined to vary between two and five minutes at this altitude. Link budget calculations were performed using these parameters to aid in equipment selection and to ensure a reliable link (at least 3 dB margin) provides sufficient data volume capability. The telecommunications link budget for downlink is provided in Table 1.

The onboard telecom components consist of an S-band transmitter and circular antenna, a UHF receiver and monopole antenna, and connective wiring, resulting in a total mass of less than 0.5 kg. The system will use Binary Phase Shift Keying (BPSK) as the form of data modulation, and the transmitting antenna can be polarized to Left-Hand-Circular (LHC) or Right-Hand-Circular (RHC) to match ground antenna polarization. This configuration will provide sufficient data rates for the communications system while limiting power consumption.

Data downlink will operate within the amateur S-band frequency range, at a frequency of 2.3 GHz. Command uplink will operate within the amateur UHF fre-

Table 1. Downlink Telemetry Budget

Parameter	Value	Units
Spacecraft		
Spacecraft Transmitter Power Output:	2.0	Watts
Spacecraft Total Transmission Line Losses:	2.2	dB
Spacecraft Antenna Gain:	2.0	dBi
Spacecraft EIRP:	2.8	dBW
Downlink Path		
Spacecraft Antenna Pointing Loss:	0.3	dB
S/C-to-Ground Antenna Polarization Loss:	1.9	dB
Path Loss:	159.2	dB
Atmospheric Loss:	1.1	dB
Ionospheric Loss:	0.2	dB
Ground Station		
Ground Station Antenna Pointing Loss:	3.3	dB
Ground Station Antenna Gain:	25.0	dBi
Ground Station Total Transmission Line Losses:	2.0	dB
Ground Station Effective Noise Temperature:	506	K
G.S. Signal-to-Noise Power Density (S/No):	61.4	dBHz
System Desired Data Rate:	30	Kbps
Telemetry System Eb/No for the Downlink:	16.6	dB
System Allowed or Specified Bit-Error-Rate:	1.0E-05	
Telemetry System Required Eb/No:	9.6	dB
Eb/No Threshold:	9.6	dB
System Link Margin:	**7.0**	**dB**

quencies at 435 MHz, at a data rate of 9600 bps, which corresponds to the limiting factors of the ground station hardware.

All telecommunications subsystem components will be provided by SpaceQuest, Inc. The S-band antenna selected is the AC-100 Circular Antenna, which will provide sufficient gain for downlink and a very wide (160°) beam width. The UHF antenna will be the ANT-100 monopole antenna, which will provide adequate gain for the low data rate uplink. The OTI satellite will also use a TX-2400 S-band transmitter, capable of operating at data rates of up to 1 Mbps and supporting 2.5 W of RF power at 800 mA. The receiver will be the RX-445 UHF receiver, which is the size of a matchbox, weighs 40 g, and is capable of 9600 bps working with Gaussian Minimum Shift Keying (GMSK) modulation. Uplink and downlink communication with the OTI spacecraft will be accomplished via the Georgia Institute of Technology Center for Space Systems tracking station.

2.7 Thermal Control

The thermal control subsystem (TCS) is required to ensure the survivability and operability of all other components by maintaining them within their allowable temperature ranges. Thermal control will be accomplished through all phases of the mission, including launch, post-launch before the satellite is powered up, safe mode, and worst-case hot and cold on-orbit environments.

The TCS is designed to be as passive as possible, to reduce the associated risk and power draw of the subsystem. The design uses multi-layer insulation, paints, coatings, heat sinks, and packaging of components to distribute heat where needed. The TCS will provide temperature monitoring of all components, with necessary redundancy using thermistors. If a component's temperature reading exceeds a critically high value, safe mode will be triggered; and if a critically low value is reached, the corresponding thermostat will activate a resistive heating element. Thermal analysis is based upon the Thermal Desktop software tool. A model with several hundred nodes has been developed for use on OTI.

3. Thermal Imaging System

The Microbolometer Thermal Imaging System consists of a UFPA and refractive optics. The UFPA is contributed by Raytheon Vision Systems, and instrument system engineering is being led by Arizona State University. Uncooled focal plane arrays are widely used in military and commercial applications (Bhan and Saxena, 2006). They have also been used for space applications, including the Thermal Emission Imaging System (THEMIS) on Mars Odyssey (Silverman and Christensen, 2006). The DARPA Orbital Express Mission also used a UFPA onboard the Autonomous Space Transport Robotic Operations (ASTRO) spacecraft. ASTRO used the UFPA to detect its sister satellite's (NextSat) thermal signature to aid in autonomous rendezvous and docking (Timmons and Ringelberg, 2008). Uncooled focal plane arrays have also flown on Earth observing missions. Examples include a 64 x 64 pixel UFPA for the Infrared Atmospheric Sound-

ing Interferometer instrument flown on the European MetOp satellites, and a 64 x 64 pixel UFPA used as a multispectral imager on the Imaging Infrared Radiometer on NASA's CALIPSO mission (Corlay, et al., 2001). Also, the New Infrared Sensor Technology (NIRST) instrument, flown as part of the SAC-D payload on the Aquarius mission, uses two 512 x 2 UFPA's as multispectral pushbroom imager. (Miklus and deCharon, 2010).

When mass and energy are limited, UFPA's provide an efficient approach to thermal imaging for small spacecraft with short development and integration times over cooled systems - provided that the reduced sensitivity is acceptable. The UFPA incorporates a sensor composed of individual microbolometer pixels and readout electronics. Each microbolometer pixel uses a radiation-absorbent material - in this case vanadium-oxide - that is sensitive to forward-looking thermal infrared radiation. The change in temperature of the absorbent material alters the electrical resistance which is in turn measured by the attached readout integrated circuit. For sensitivity, it is important that the absorbent material is thermally isolated from the rest of the integrated circuit to ensure reliability. Micromachining techniques allow these absorbent materials to be suspended micrometers above the rest of the device. This allows the absorbent material to be thermally isolated from the read-out integrated circuit, negating the need for active cooling.

The UFPA used by the OTI mission is the OWL IR-640, produced by Raytheon Vision Systems (RVS) (Raytheon data sheet, 2010), previously used for helmet-mounted infrared imagers. The specifications for the UFPA can be seen in Table 2. A photo of the UFPA is shown in Figure 4. The UFPA will be paired with a commercial infrared lens from Ophir Optronics to form the microbolometer thermal imaging system.

The microbolometer thermal imaging system will measure light at 8-12 microns. The microbolometer pixels are stabilized to within ±0.1 K using an integrated Thermal Electric Cooler. The absolute accuracy of the thermal imaging system is expected to be ±2 K, based on calibration experience with THEMIS. A calibration flag is imaged as a reference black body before and after taking an image of the scene, in order to measure and mitigate any drift that may occur between measurements. Any drift will be measured and subtracted out of the image. For the OTI mission, identification of warm-water ocean features associated with currents requires the capability to discern relative temperature differences within a scene; the thermal imaging system is an ideal instrument for this application. The effects of atmospheric attenuation can be assumed to be constant for a given scene, so any variations caused by the attenuation will not affect the differentiation of thermal feature detection required for the mission.

Table 2. Thermal Imaging System Operating Specifications

Parameter	Value
Overall Mass (kg)	1.73
Peak Power Dissipation (W)	2
Spatial Resolution (m) from 500km altitude	124
Noise-Equivalent Differential Temperature (mK) @ F/1.0, 25°C, 30 Hz 60	60
Pixel Pitch (μm)	25
Spectral Range (μm) from 500km altitude	8 to 12
Frame Rate (Hz)	40
Field of View	9.1° x 6.8°
Ground Footprint (km) from 500km altitude	79 x 60
Array Size (pixels)	640 x 480

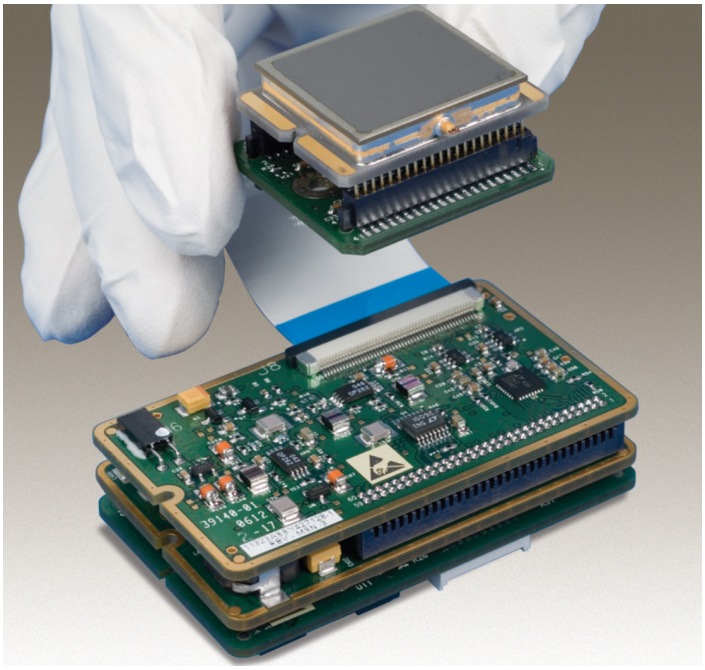

Figure 4. Raytheon Vision Systems OWL IR-640 (Credit: Raytheon).

4. Thermal Image Processing

Image processing algorithms have been tested using images from the Advanced Spaceborne Thermal Emission and Reflection Radiometer (ASTER) instrument on board the Terra satellite (Yamaguchi et al., 1998). Terra is one of the flagships of the Earth Observing System of satellites. Thermal images from ASTER have a spatial resolution of 90 m pixel^{-1}, providing a suitable proxy for the anticipated OTI images at 124 m pixel^{-1}. The OTI microbolometer thermal imaging system and the Thermal Infrared (TIR) subsystem of ASTER are similar, since they both observe the Thermal Infrared region (8-12 microns). However, ASTER is a multispectral, scanning, cryocooled imager, while the OTI microbolometer thermal imaging system is a broadband, framing, uncooled imager. ASTER also has SWIR (ShortWave Infrared) and VIR (Visible Near Infrared) subsystem components. A sample ASTER image showing the Gulf Stream off the coast of Cape Hatteras, North Carolina (39.2° N, 75.5° W) is shown in Figure 5. In this thermal image, the warmer waters of the Gulf Stream are apparent in the lower right of the image. Coastal eddies adjacent to the Cape are also discernable. This image will be used to test and demonstrate the capacities of the "blobber" algorithm.

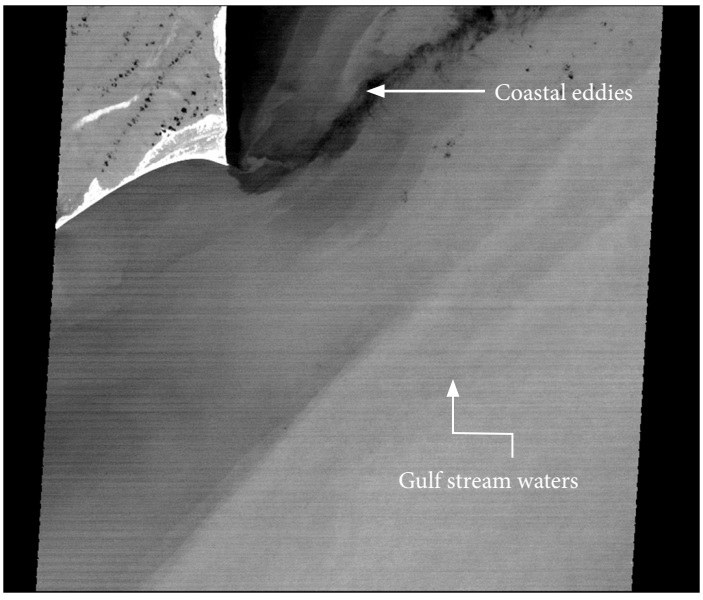

Figure 5. ASTER surface kinetic temperature image showing the Gulf Stream near Cape Hatteras, NC. Wavelengths between 8 – 12 μm, radiometric accuracy of 1K for each of the five bands (Gillespie et al., 1999).

A "blobber" algorithm is used by the OTI mission to identify a set of contiguous pixels with characteristics that fall within specified temperature and area parameters. Previous versions of blobber algorithms have been used for space-based autonomous infrared image processing applications. The Deep Impact spacecraft employed a blobber algorithm to autonomously navigate the Deep Impact spacecraft onto a collision course with the nucleus of comet Tempel-1 (Mastrodemos, et al., 2005). The DARPA Orbital Express mission used microbolometer-based thermal images for autonomous rendezvous and docking of twin satellites (Timmons and Ringelberg, 2008). The OTI mission will be the first application of on-board image processing of thermal images for near real-time ocean thermal feature monitoring. The blobber algorithm has been developed at Georgia Tech using MATLAB™, and transferred into C code for use on the flight processor. Initial system testing has demonstrated that the algorithms run successfully on the flight processor. Ground-based post-processing of selected images is also planned prior to publication of flight images and incorporation into an internet-based system for tracking ocean surface thermal features.

The blobber algorithm is capable of detecting contiguous sets of pixels (blobs) within a specified range of intensity. A threshold on the allowable area of the blob is used to screen candidate sets of contiguous pixels based on their combined area, allowing selection of blobs within prescribed size limitations. The OTI mission will use the blobber algorithm to isolate thermal features based on surface temperature differentials with the surrounding waters. Surface thermal features can be broadly distributed for large-scale ocean circulation structures, or localized for river outflows and shoreline-generated eddies. This application is useful for the validation of numerical mesoscale and sub-mesoscale current modeling and long-term weather forecasting. The near real-time geolocation of warm-water ocean current features can be used by the oceanographic science community in the planning of cruises for collection of in-situ observations. Ocean currents monitoring also has direct application to energy efficiency of maritime operations.

The blobber algorithm begins with a matrix repre-

sentation of a thermal image, with each element having an intensity value between 0 and 255. The intensity value of each pixel is an 8-bit representation of the scene viewed by the associated element in the focal plane. The dimensions of the matrix are determined by the size of the focal plane, i.e. 640 x 480 pixels.

The blobber algorithm initially scans the image, and creates a second matrix (called *intens_screen*) that assigns a value of 255 to a cell if the corresponding pixel intensity from the thermal image falls within the selected intensity range. Pixels with intensities outside of the desired range are assigned a value of zero in the *intens_screen* matrix. From the Cape Hatteras image, pixels that meet the expected intensity range from the Gulf Stream are shown as white pixels in Figure 6. When a thermal image is acquired, the average intensity of the image is found. The minimum intensity screen for the blobber algorithm is set to be equal to the average intensity in the scene. The maximum intensity screen for the blobber algorithm is set to the average scene intensity plus 3 sigma. The intensity range threshold used in generating Figure 6 is 127 - 247, corresponding to a temperature range of 302.5 - 308.3 K. It is noted that both land and water areas are contained within the specified intensity range.

The next step in the blobber algorithm identifies sets of contiguous pixels within the specified area range. The *intens_screen* matrix is scanned, and each pixel that has a value of 255 and that has a nearest neighbor with a value of 255 in the *intens_screen* matrix is retained; isolated pixels are assigned a value of zero. The resulting matrix (called *in_blob*) contains blobs of contiguous pixels within the specified intensity threshold. Individual blobs are then numbered. This is accomplished through scanning the *in_blob* matrix, assigning integer numbers to the blob elements and incrementing the value each time a new blob is encountered. Results are written to a file called *blob_number*. Depending upon the geometry of the blobs, the first pass through the image may result in more than one blob number being assigned to elements within the same blob. A second pass through the image is then made. For each numbered pixel within a blob, all adjacent pixels that are part of the blob are queried, and the minimum blob number from the adjacent pixels is retained. This step is repeated until there are no further changes in the *blob_number* matrix. The blobber algorithm then calculates the area of the blobs that have been found, through counting the number of pixels within each blob. An area threshold is applied, retaining only those blobs having a number of pixels within a specified range. The result of this process as implemented on the Cape Hatteras image is shown in Figure 7. Note that the area screen within the blobber algo-

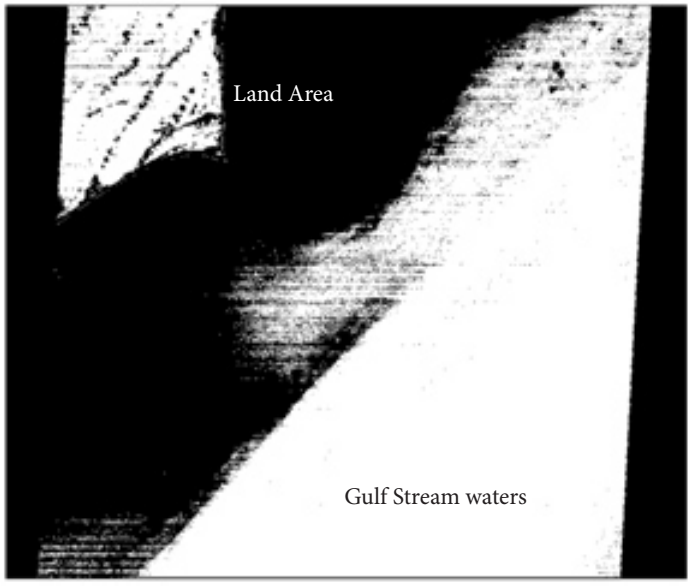

Figure 6. Pixels from Cape Hatteras image within specified intensity range.

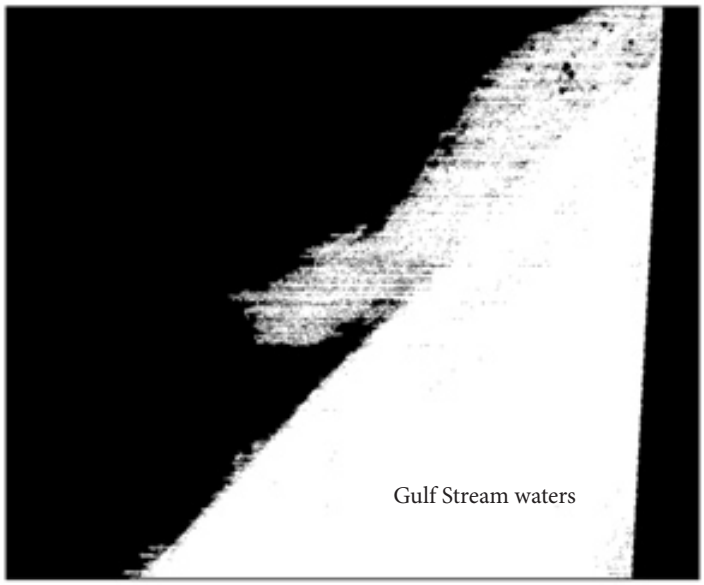

Figure 7. Area screening is used to isolate ocean thermal features.

rithm operates based upon pixel counts; the geometric area covered by each blob in the earth-based scene is a function of the orbit altitude and instrument pointing angle. Area screening allows the elimination of the land mass seen in the top left of Figures 5 and 6. The expected area of the land mass within the targeted image is calculated as part of the science mission planning process; the acceptable area range for the ocean current feature is selected based upon the expected water-to-land ratio for the planned image. For planned image targets where the field of view encompasses roughly equivalent land and water areas, the area screen is relaxed and the intensity screen is used to discriminate between land and water blobs.

The blobber algorithm can effectively remove clouds during image processing. Figure 8 shows an ASTER infrared image containing clouds near the coast of South Carolina. The clouds are dramatically colder than the warm-water ocean currents, and are removed during image processing via the blobber algorithm intensity screen. However, clouds may obscure the desired current features, causing voids in the output data products. Repeated imaging of current features is necessary to fill voids and monitor the ocean current evolution with time.

Figure 8. Clouds may be screened from processed images based upon pixel intensity.

For some applications, calculation of the center of brightness of the identified blob is desired. Analogous to a center of mass calculation, the formulation used for center of brightness is shown in Equations 1 and 2, below. Row and column coordinates are represented by i and j, respectively. The formulation leads to a center of brightness location that is biased toward the high-intensity area of the thermal feature. Note that the center of brightness is not constrained to be located on a pixel within the blob; for unusual blob distributions, the center of brightness may fall outside of the blob contiguous area.

$$x_{cob} = \frac{\Sigma_{i,j} i \times \text{intens}(i,j)}{\Sigma_{i,j} \text{intens}(i,j)} \quad (1)$$

$$y_{cob} = \frac{\Sigma_{i,j} j \times \text{intens}(i,j)}{\Sigma_{i,j} \text{intens}(i,j)} \quad (2)$$

5. Image Geolocation

Once the thermal image processing algorithms have identified image pixels associated with warm-water ocean currents, on-board orbit determination and attitude vectors are used to determine the latitude/longitude coordinates of the thermal feature. A closed-form approach for determining where a body-fixed vector intersects an ellipsoid approximating the Earth's surface is applied (Patt and Gregg, 1994). The surface ellipsoid is defined by an equatorial radius, r_e, of 6378.137 km, and a polar radius $r_p=r_e(1-f)$ where the flattening factor is f=1/298.257.

The OTI spacecraft is equipped with a global positioning system receiver, which provides orbit state information (position and velocity). Spacecraft attitude knowledge is provided by a star tracker. Orbit state and attitude data are filtered and interpolated to the epoch at which the image was acquired. The spacecraft position vector relative to the Earth's center, S, is transformed to the Earth Mean Equator and Prime Meridian of Date coordinate system, which is a rotating, Earth-centered reference frame. In this frame, the **X** unit vector is in the direction of the prime meridian, the **Z** unit vector is

orthogonal to the mean equator of date in the direction of Earth's rotation, and **Y** completes the right-handed system.

The "look" unit vector, **L**, associated with the center of each pixel in the microbolometer thermal imaging system's field of view (or, alternatively, the pixel vertices) is known, in body-fixed coordinates. The look unit vectors for the pixels contained within the thermal features in processed images are transformed to the Earth Mean Equator and Prime Meridian of Date coordinate frame for geolocation. The magnitude of the vector L is the distance from the spacecraft to the Earth ellipsoid along the look vector; this distance must be determined.

A given look vector will intersect the Earth's surface at a distance from the Earth's center defined by the Earth ellipsoid. The vector **G** is defined as the vector from the Earth's center to the location where the look vector intersects the Earth's ellipsoid. Since the components of **G** are known to lie on the ellipsoid, it is apparent that:

$$\left(\frac{G_1}{r_e}\right)^2 + \left(\frac{G_2}{r_e}\right)^2 + \left(\frac{G_3}{r_p}\right)^2 = 1 \tag{3}$$

where G_1, G_2, and G_3 are the components of the vector **G** in the Earth Mean Equator and Prime Meridian of Date frame.

Because all three vectors are defined in the same coordinate frame, vector addition yields:

$$\mathbf{S} + \mathbf{L} = \mathbf{G} \tag{4}$$

The known spacecraft position vector **S** can be expressed as

$$\mathbf{S} = S_1\mathbf{X} + S_2\mathbf{Y} + S_3\mathbf{Z} \tag{5}$$

Similarly, the look vector **L** can be expressed as

$$\mathbf{L} = L(l_1\mathbf{X} + l_2\mathbf{Y} + l_3\mathbf{Z}) \tag{6}$$

where L is the look vector magnitude that must be determined, and l_1, l_2, and l_3 represent the known components of the look unit vector. Combining equations (4), (5) and (6), the components of **G** can be written as

$$G_1 = S_1 + L \times l_1 \tag{7a}$$

$$G_2 = S_2 + L \times l_2 \tag{7b}$$

$$G_3 = S_3 + L \times l_3 \tag{7c}$$

Substituting equations (7) into (3) yields

$$\left(\frac{S_1 + L \times l_1}{r_e}\right)^2 + \left(\frac{S_2 + L \times l_2}{r_e}\right)^2 + \left(\frac{S_3 + L \times l_3}{r_p}\right)^2 = 1 \tag{8}$$

Expanding equation (8) and grouping terms yields Equation 9, shown below as Figure 9. Equation (9) is a quadratic equation that can be solved for L. All other terms in Equation (9) are known. Note that when solving the quadratic equation, the smaller value of the two solutions is selected. Equation (7) can now be evaluated, and the vector from the Earth's center to the location on the ellipsoid where the look vector intersects can be written as

$$\mathbf{G} = G_1\mathbf{X} + G_2\mathbf{Y} + G_3\mathbf{Z} \tag{10}$$

The geocentric latitude associated with **G** can be found using the relationship:

$$\tan(lat_c) = \frac{G_3}{\left(G_1^2 + G_2^2\right)^{1/2}} \tag{11}$$

$$\left[l_1^2 + l_2^2 + l_3^2\left(\frac{r_e}{r_p}\right)^2\right]L^2 + \left[2l_1S_1 + 2l_2S_2 + 2l_3S_3\left(\frac{r_e}{r_p}\right)^2\right]L + \left[S_1^2 + S_2^2 + S_3^2\left(\frac{r_e}{r_p}\right)^2 - r_e^2\right] = 0$$

Figure 9. Equation (9).

and the geodetic latitude can be computed from:

$$\tan(lat_d) = \frac{\tan(lat_c)}{(1-f)^2}. \quad (12)$$

Longitude can be found using:

$$\tan(lon) = \frac{G_2}{G_1}. \quad (13)$$

Quadrant checks must be applied when taking the inverse tangents to find latitude and longitude. Through this method, the geodetic coordinates associated with each pixel contained within the thermal feature of interest are determined.

The accuracy of the thermal feature geolocation process is dependent upon the orbit determination uncertainty and spacecraft attitude knowledge errors. A geolocation error budget will be developed for the

OTI mission during the detailed design phase. System performance will be assessed during the spacecraft checkout phase, shortly following launch. Coastal images showing identifiable land masses with known coordinates will be used to calibrate the on-board geolocation process.

6. Conclusion

The OTI mission will demonstrate autonomous thermal image processing and geolocation of images in low-Earth orbit. This capability is applicable to a broad range of potential applications, including space situational awareness, wildfire monitoring, and military surveillance. OTI will apply the capability to the monitoring of ocean thermal features associated with warm-water currents. Science data resulting from the OTI mission will allow the publication of an ocean current database with daily updates, enabling improvements to weather forecasting, climate modeling, and maritime operations efficiency. The mission is designed to geolocate the boundaries warm-water ocean currents to a spatial accuracy of 1 km. Initial evaluation of system capabilities indicate that the geolocation requirement will be met.

Uncooled focal plane arrays provide a resource-efficient means for obtaining thermal imagery from orbit. The OTI investigation will advance the orbital use of UFPAs by characterizing the radiation environment effects on the imager throughout the six-month mission.

On-board processing of thermal images will be accomplished through the use of the blobber algorithm, which screens the images for groups of pixels meeting constraints for intensity and area. Using spacecraft attitude and orbit information, the images are geolocated, resulting in the capability to autonomously calculate the geodetic coordinates of thermal features. Limitations of the blobber algorithm include a small temperature difference between the current with respect to the surrounding waters or a cloud obstruction of the region of interest. These limitations can be improved with a frequent overpass of the targeted currents.

Acknowledgments

The OTI mission is a student-led effort managed by the Georgia Institute of Technology Center for Space Systems, with instrument system engineering provided by the School of Earth and Space Exploration at Arizona State University. The OTI UFPA was contributed by Raytheon Vision Systems. The OTI mission design leverages work done in support of prior missions that were funded by the University Nanosatellite Program, sponsored by the Air Force Office of Scientific Research and the Air Force Research Laboratory.

References

Bhan, R. and Saxena, R. (2009): Uncooled infrared microbolometer arrays and their characterization techniques, *Defense Science J.*, 59, No. 6, 580-589.

Corlay, G., et al. (2001): Microbolometer in space: IASA and PICASSO-CENA, *Acta Astronautica,* 48, No. 5-12, pp. 299-309.

Davidson, F. J. M., et al. (2009): Applications of GODAE ocean current forecasts to search and rescue and ship routing, *Oceanography*, 22, No. 3, pp. 176-181.

Gillespie, A. R., et al. (1999): Temperature/- emissivity separation algorithm theoretical basis document, Version 2.4. NAS5-31372, NASA/GSFC, Greenbelt, MD.

Leben, R. R. and Born, G. H. (1993): Tracking loop current eddies with satellite altimetry, *Advances in Space Research*, 13, Iss. 11, pp. 325-333.

Mastrodemos, N., et al. (2005): Autonomous navigation for the deep impact mission encounter with Comet Tempel 1, *Space Science Reviews*, 117, Iss. 1, pp. 95-121.

Miklus, N. and deCharon, A. (2010): Aquarius/SAC-D, sea surface salinity from space mission brochure. Available: http://aquarius.nasa.gov/pdfs/Aquarius_Mission_Brochure_508_Compliant.pdf

Patt, F. S. and Gregg, W. W. (1994): Exact closed-form geolocation algorithm for Earth survey sensors, Int. *J. Remote Sensing*, 15, No. 18, pp. 3719-3734.

Point Grey Research® Inc. Grasshopper™ Technical Reference Manual Version 1.1 (2008). Available http://www.ptgrey.com/products/grasshopper/grasshopper_firewire_camera.asp

Raytheon OWL IR-640 data sheet (2010): IMS 04/10 DTS09-1072.

Raytheon 640 × 512/480 (U640) Uncooled focal plane assembly data sheet (2008): IMS 01/08 DTS08-0197

Silverman, S. and Christensen, P. (2006): Successful Mars remote sensors, MO THEMIS and MER Mini-TES, *Acta Astronautica,* 59, pp. 8-11.

Timmons, K. and Ringelberg, J. (2008): Approach and capture for autonomous rendezvous and docking, in Proc. *2008 IEEE Aerospace Conf.*, Big Sky, MT.

Walker, L. and Spencer, D. (2010): R3: Thermal imaging and rapid feature detection for small satellites. AIAA-RS8-2010-3002, 8th Responsive Space Conference, Los Angeles, CA.

Yamaguchi, Y., et al. (1998): Overview of Advanced Spaceborne Thermal Emission and Reflection Radiometer (ASTER), in *IEEE Trans. Geoscience and Remote Sensing,* 36, Iss. 4, pp. 1062-1071.